Flow Turbulence Combust (2009) 83:407–423
DOI 10.1007/s10494-009-9228-9

Numerical Study of n-Heptane Auto-ignition Using LES-PDF Methods

W. P. Jones · S. Navarro-Martinez

Received: 30 September 2008 / Accepted: 21 May 2009 / Published online: 5 June 2009

Abstract This work deals with pre-vaporized n-heptane auto-ignition in turbulent flows. The paper applies the Eulerian Stochastic Field method to the solution of the sub-grid joint-scalar probability density function (PDF) of the reacting scalars in the Large Eddy Simulations (LES) context. A reduced mechanism of 22 species and 18 reactions is used to model n-heptane chemical kinetics. The method is able to reproduce the different regimes observed experimentally and studies the influence of inflow temperature fluctuations.

Keywords LES-PDF · Auto-ignition · Heptane

1 Introduction

The renewed interest in "cleaner" modes of diesel combustion, such as homogeneous charge compression ignition (HCCI) and lean premixed pre-vaporized (LPP) engines motivates the increase in auto-ignition research to develop accurate predictive tools, especially in transient regimes. A great deal of research has been performed in homogeneous ignition systems; however there are few studies in the inhomogeneous mixtures typical of diesel ignition. Moreover, the results obtained to date have been contradictory; some experiments [1] suggest that increased turbulence levels delay auto-ignition, whilst Direct Numerical solutions (DNS) results [2] predict the opposite, with shorter ignition times.

Ignition problems are particularly difficult to model due to the fact that fluid mechanical and chemical time scales are of the same magnitude. Current understanding

W. P. Jones · S. Navarro-Martinez (✉)
Department of Mechanical Engineering, Imperial College London,
Exhibition Road, London SW7 2AZ, UK
e-mail: s.navarro@imperial.ac.uk

W. P. Jones
e-mail: w.jones@imperial.ac.uk

of auto-ignition in turbulent flows is limited by the difficulty in making detailed measurements and because computer limitations prevent the application of DNS of the equations of motion to compute turbulence-chemistry interactions at realistic Reynolds numbers. Moreover, for large molecule hydrocarbons, a large number of species need to be considered, as "slow" reactions are important in the formation of a pool of reactants, mainly radicals R-HO_2 and R-H_2O_2, which act as a trigger for combustion. The inclusion of these intermediates greatly increase the computational cost of such calculations. In addition the ignition process is initiated in lean premixed mixtures and propagates into richer conditions, [3], exhibiting a behavior midway between premixed and non-premixed flames (often called "partially" premixed [4]). The combustion of lean hydrocarbon mixtures is very sensitive to conditions existing in the oxidizer stream and therefore auto-ignition characteristics are expected to depend strongly on the air temperature and turbulence.

There are not many turbulence-combustion models able to target auto-ignition systems due to the combination of are highly time-dependent solution and partially premixed regime. Large Eddy Simulation (LES) has a considerable potential to represent time-dependent turbulent combustion with substantial advantages over Reynolds averaged Navier-Stokes (RANS) models. Although combustion is mainly a sub-grid phenomenon, LES ability to produce accurate predictions of the mixing scalar fields greatly benefits numerical simulations in combustion. LES models for turbulence combustion are often based on RANS counterparts and are commonly divided along the lines of non-premixed and premixed regimes. Examples of LES combustion applications in non-premixed combustion are fast-chemistry and equilibrium chemistry [5, 6], flamelets [7], Conditional Moment Closure [8] while in premixed combustion flame-surface density models [9] and G-equation [10, 11] among others (see Pitsch [12] for a comprehensive review of LES combustion models). The above regime distinction is not adequate for auto-ignition problems which exhibit an "hybrid" behavior and moreover they require a chemical time evolution to distinguish between "slow" intermediate reaction and "fast" reactions. The one-point joint filtered probability density function *pdf* [13] for all the scalars quantities needed to describe the reaction provides a means of predicting the filtered fields of reactive species independent of the combustion regime The main disadvantage of the *pdf* approach is the high dimensionality of the system, especially when many scalars are considered, which makes the problem only tractable with stochastic solution methods. The most common adopted approach to solving the *pdf* evolution equation is by using large number of stochastic particles which are used to represent the joint-PDF. This approach is denoted "Lagrangian" and example applications in LES are [14, 15]. Recently, new methods of solving the *pdf* transport equation in a fully Eulerian manner have been developed [16, 17]. These methods are based on stochastic Eulerian fields, which evolve according to stochastic partial differential equations and , like stochastic particles, they represent the joint-PDF of the reactive scalars. The stochastic fields method is easy to implement in existent CFD codes as there are no interpolation procedures and therefore they are faster than Lagrangian ones with the same number of samples per cell. Previous work on LES with the stochastic field method can be found in [18, 19].

Numerical studies of auto-ignition have been centred mainly in auto-ignition as a stabilization mechanism. The most numerous examples are in lifted flames with vitiated co-flow, where RANS [20–22] and LES [19, 23, 24] amongst others, where

able to obtain good agreement with measured data. However, in non-stationary auto-ignition there are fewer RANS examples [25, 26] as RANS-type models are incapable of providing the transient information required to reproduce auto-ignition phenomena. However, to date there appear to have been few LES investigations of auto-ignition [27, 28] and none for complex hydrocarbons. The current work seeks to provide a better understanding of transient n-heptane auto-ignition, especially the effects of temperature and turbulent fluctuations. n-heptane is widely used as a research fuel due to its similarities to diesel fuel (they have very similar cetane number).

2 Mathematical Formulation

In LES a spatial filter is applied to the equations of motion: the spatial filter of a function $f = f(\mathbf{x}, t)$ is defined as its convolution with a filter function, G, according to:

$$\overline{f}(\mathbf{x}, t) = \int_{\Omega} G(\mathbf{x} - \mathbf{x}'; \Delta(\mathbf{x}))\, f(\mathbf{x}', t) d\mathbf{x}' \tag{1}$$

where the filter function must be positive definite in order to maintain filtered values of scalars such as mass fraction within bound values and to preserve the nature of the chemical sources terms (a filter that changes sign may change consumption terms to formation type terms). The integration is defined over the entire flow domain Ω and the condition that the filter kernel G should be positive definite implies that it has the properties of a *pdf*. The filter function has a characteristic width of Δ which, in general, may vary with the position. The density variations in the unresolved scales that arise in combusting flows can be treated through the use of density weighted, or Favre, filtering, defined by $\tilde{f}(\mathbf{x}, t) = \overline{\rho f}/\overline{\rho}$. Application of the density weighted filtering operation to the equations of motion results in:

Continuity

$$\frac{\partial \bar{\rho}}{\partial t} + \frac{\partial \bar{\rho} \tilde{u}_i}{\partial x_i} = 0, \tag{2}$$

Momentum

$$\frac{\partial \bar{\rho} \tilde{u}_i}{\partial t} + \frac{\partial \bar{\rho} \tilde{u}_i \tilde{u}_j}{\partial x_j} = -\frac{\partial \bar{p}}{\partial x_i} + \frac{\partial}{\partial x_j}\left(2\mu \bar{S}_{ij}\right) - \frac{\partial}{\partial x_j}\tau_{ij} \tag{3}$$

where $\bar{S}_{ij}$ is the resolved rate of strain tensor. The deviatoric part of the sub-grid scale stress tensor $\tau_{ij} = \overline{\rho}\left(\widetilde{u_i u_j} - \tilde{u}_i \tilde{u}_j\right)$ is determined with the Smagorinsky model [29] :

$$\tau_{ij}^{d} = 2\mu_{sgs}\tilde{S}_{ij}$$

with

$$\mu_{sgs} = \overline{\rho}\left(C_S \Delta\right)^2 ||\tilde{S}_{ij}||$$

where $||\tilde{S}_{ij}|| \equiv \sqrt{2\tilde{S}_{ij}\tilde{S}_{ij}}$ is the Frobenius norm of the resolved rate of strain tensor. The filter width is taken as the cube root of the local grid cell volume and the

parameter C_S is obtained through the dynamic procedure of Piomelli and Liu [30]. The isotropic part of the viscous and sub-grid stress has been adsorbed into the pressure.

2.1 Filtered probability density function

Using the filtering operation, (1) and following Gao and O'Brien [13] a density weighted sub-grid (or filtered) *pdf* for the N_s scalar quantities needed to describe reaction can be defined:

$$\tilde{P}_{sgs}\left(\underline{\psi};\mathbf{x},t\right)=\int_{\Omega}\frac{\rho(\mathbf{x}')}{\bar{\rho}}\mathcal{F}\left(\mathbf{x}'\right)G\left(\mathbf{x}-\mathbf{x}',\Delta\right)d\mathbf{x}'. \tag{4}$$

where $\mathcal{F}\left(\underline{\psi};\mathbf{x},t\right)=\prod_{\alpha=1}^{N_s}\delta\left(\psi_\alpha-\phi_\alpha\left(\mathbf{x},t\right)\right)$ is a fine-grained *pdf*.

An exact evolution equation for this quantity can then be derived, *e.g.* [13, 31, 32], from the appropriate conservation equations by standard methods. The result is:

$$\begin{aligned}\overline{\rho}\frac{\partial\widetilde{P}_{sgs}(\underline{\psi})}{\partial t}+\overline{\rho}\tilde{u}_j\frac{\partial\widetilde{P}_{sgs}(\underline{\psi})}{\partial x_j}+\sum_{\alpha=1}^{N_s}\frac{\partial}{\partial\psi_\alpha}\left[\overline{\rho}\dot{\omega}_\alpha(\underline{\psi})\widetilde{P}_{sgs}(\underline{\psi})\right]=\\ -\frac{\partial}{\partial x_i}\left[\Gamma\frac{\partial\tilde{P}_{sgs}(\underline{\psi})}{\partial x_i}\right]\\ -\sum_{\alpha=1}^{N_s}\sum_{\beta=1}^{N_s}\frac{\partial^2}{\partial\psi_\alpha\partial\psi_\beta}\left\{\left(\frac{\mu}{\sigma}\overline{\frac{\partial\phi_\alpha}{\partial x_i}\frac{\partial\phi_\beta}{\partial x_i}\middle|\underline{\phi}=\underline{\psi}}\right)P_{sgs}(\underline{\psi})\right\}\end{aligned} \tag{5}$$

where equal diffusivities have been assumed and the spatial and temporal dependency of the *pdf* have been dropped for compactness. In (5) a gradient model [33] has been used to model the *pdf* transport by sub-grid turbulent fluctuations. The transport coefficient is given by $\Gamma=\frac{\mu}{\sigma}+\frac{\mu_{sgs}}{\sigma_{sgs}}$ where σ_{sgs} is a constant *sgs* Prandtl/Schmidt number assigned the value 0.4 [7, 8].

The final 'micro-mixing' term in (5) represents the effect of molecular diffusion on the sub-grid *pdf*. There are several models available for this term although none of them entirely satisfactory (see [34] and references therein for reviews). In the present work, following previous works by Mustata et al. [18] and Jones and Navarro-Martinez [19] the IEM/LMSE closure [35–37], is adopted for use in LES. Thus the final term in (5) is replaced by:

$$\frac{\overline{\rho}}{\tau_{sgs}}\sum_{\alpha=1}^{N_s}\frac{\partial}{\partial\psi_\alpha}\left[\left(\psi_\alpha-\phi_\alpha(\mathbf{x},t)\right)\tilde{P}_{sgs}(\underline{\psi})\right]$$

where the *sgs* mixing time scale is given, [38], by,

$$\tau_{sgs}^{-1}=C_d\frac{\mu+\mu_{sgs}}{\bar{\rho}\Delta^2}$$

with the micro-mixing constant assigned the value $C_d=2$.

2.2 The LES-stochastic field formulation

The stochastic field solution method is based on deriving a system of stochastic partial differential equations (spdes) equivalent to the closed form of the *pdf* equation (5). The stochastic fields, resulting from the solution of the spdes, are defined in the whole space. They do not correspond to any 'realisation' of the turbulent flow field but, rather, represent an equivalent stochastic system with the same one-point *pdf* as (5). The density weighted *pdf* is represented by an ensemble, N of stochastic fields $\xi_\alpha^n(\mathbf{x}, t)$ such that:

$$\tilde{P}_{sgs}(\underline{\psi}; \mathbf{x}, t) = \frac{1}{N}\sum_{n=1}^{N}\prod_{\alpha=1}^{N_s}\delta[\psi_\alpha - \xi_\alpha^n(\mathbf{x}, t)] \tag{6}$$

Filtered values are then simply obtained by averaging

$$\tilde{\phi}_\alpha = \frac{1}{N}\sum_{n=1}^{N}\xi_\alpha^n$$

The exact derivation of the spdes lies beyond the scope of this paper. Two approaches exists: that of Valiño [16] which involves an Ito interpretation of the stochastic integral and that of Sabel'nikov and Soulard [17] where a Stratonovich interpretation of the integral is adopted. The latter approach preserves the results of classical differential calculus. Previous calculations by the authors suggest that mass errors are somewhat smaller using the Stratonovich approach and sub-grid *pdfs* are narrower. However, this difference is more likely due to the numerical implementation adopted rather than to the formulation itself. In the present work a Stratonovich formulation is used and the equation for the stochastic fields is then given by:

$$\bar{\rho}\frac{\partial \xi_\alpha^n}{\partial t} + \bar{\rho}\left(\tilde{u}_j + u_j^g + u_j^d\right)\frac{\partial \xi_\alpha^n}{\partial x_j} = \frac{\bar{\rho}}{\tau_{sgs}}\left(\xi_\alpha^n - \tilde{\phi}_\alpha\right) + \bar{\rho}\dot{\omega}_\alpha(\underline{\xi}^n) \tag{7}$$

where u_j^g is a stochastic velocity defined as:

$$u_j^g = \sqrt{\frac{2\Gamma}{\bar{\rho}}} \circ \frac{dW_j^n}{dt} \tag{8}$$

and where dW_j^n represent increments of a Wiener process, different for each stochastic field, n but independent of the spatial location $\mathbf{x}$ and $\circ$ denotes the Stratonovich interpretation of the stochastic integral [39]. The Wiener process is approximated by time-step increments $\mathrm{d}t^{1/2}\eta_i^n$, where η_i^n is a $\{-1, 1\}$ dichotomic random vector, [40] The drift velocity u_j^d is given by:

$$u_j^d = \frac{1}{2}\frac{\partial \Gamma/\bar{\rho}}{\partial x_j} - \frac{1}{\bar{\rho}}\frac{\partial \Gamma}{\partial x_j} \tag{9}$$

3 Experimental and Numerical Setup

The case considered in the present work corresponds to the configuration studied experimentally by Markides et al. [41, 42]. It consists of a central jet of gaseous fuel

(vaporised n-heptane/nitrogen) issuing into a stream of pre-heated turbulent air in a duct flow.

Several air and jet velocities were investigated in the experiments. In the present calculations the case of equal bulk velocities $V_{jet} = V_{air} = 18$ m/s is studied with nominal air temperatures, T_{air}, between 1130 and 1165 K (see Table 1).

The turbulent co-flow is generated by a perforated plate with 3 mm holes and 44% solidity. The experiments show a well developed turbulent spectrum in the co-flow with $u'/V_{air} = 0.12$–0.15, relatively uniform across the pipe. Assuming isotropic turbulence, the Kolmogorov length-scale was estimated $\eta \approx 0.1$–0.2 mm (see Markides et al. [42]). An estimate of the integral length scale of $L_{turb} \approx 3$–4 mm was obtained from Taylor's hypothesis with a turbulent timescale of 1–2 ms. Due to the pre-heated co-flow, the system is at relatively low turbulent Reynolds number, $Re_{turb} = u' L_{turb}/\nu$, which varied between 50 and 100. The central jet has a diameter of 2.25 mm (smaller than L_{turb}) and the considered test section computed in the present work is 125 mm. Auto-ignition was detected experimentally by chemiluminescence of the hydroxyl radical (OH*). The in house code BOFFIN [43] was used for the computations to be reported. It utilizes a second-order-accurate finite volume method, based on a fully implicit low-Mach-number formulation. The version applied utilized a staggered storage arrangement. For the momentum equation convection terms an energy-conserving discretization scheme is used and all other spatial derivatives are approximated by standard second-order central differences. As is common practice [7, 44], a total variation diminishing (TVD) scheme [45] is used for the scalars to avoid unphysical overshoots and second law violations.

The cylindrical grid consists of $256 \times 72 \times 48$ cells in the axial, radial and azimuthal directions respectively. The radial mesh size Δr varies between 0.1 and 0.4 mm and the axial spacing Δx between 0.4 and 0.6 mm. The filter width in the bulk flow is of the order of η and it was considered that the LES resolution was sufficient away from the pipe walls. 8 stochastic fields were used for the PDF solution, following previous calculations on Hydrogen auto-ignition in the same configuration [28]. To reproduce the turbulence generated by the metallic grid, a database of turbulent velocity $u_j(r, \theta; t)$ was generated with the digital filters approach of [46] and used as inflow boundary condition. This technique creates correlated structures in time and space, (see Fig. 1), using the experimentally measured length and time scales ($L_{turb} = 3$ mm and $\tau_{turb} = 1$ ms).

To introduce temperature fluctuations, the following assumption is made

$$\frac{T'}{T_{air}} = C_T \frac{\sqrt{k_{sgs}}}{V_{air}} \tag{10}$$

where C_T is adjusted depending on the level of $T' \equiv sqrt(T - T_{air})^2$ desired and $k_{sgs} = \frac{1}{2}(u_j^* - V_{air})^2$, where $\mathbf{u}^*$ is extracted from a similar database to the one used

Table 1 Case studied with parameters used

	T_{air} (K)	T' (K)	Observations
Case 1	1135	0,15,30	No burning
Case 2	1150	0,15,30	Random spots
Case 3	1155	0	Random spots
Case 4	1165	15	Flash-back

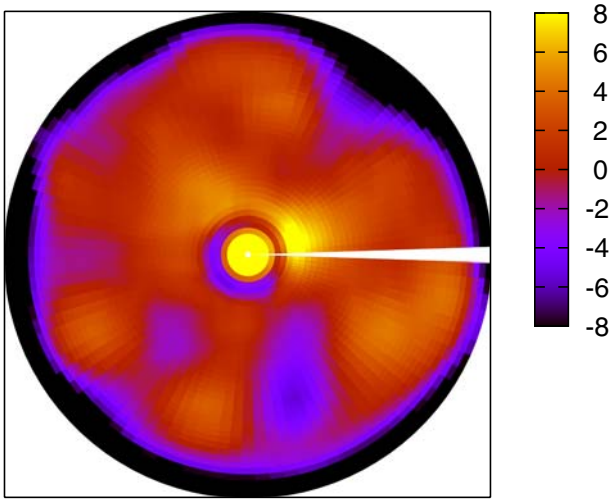

Fig. 1 Example of inflow axial velocity fluctuations $V - Vair$. The *dark areas* represent the lateral boundary layers

as turbulent inflow. This process implicitly assumes that length scales of temperature and velocity fluctuations, L_{turb}, are equal. Experimentally the RMS of temperature was measured $T' \approx 2.5$ K, however it must be noted that T_{air} has an indeterminate uncertainty of $\pm 0.3\%$ and a determinate uncertainty of $\pm 0.6\%$ (7 K). Further conduction losses (not considered here) result in a reduction in the temperature by about 10 K in the first 100 mm [47]. In this work two values of T' have been used, 15 K and 30 K, which correspond to values of C_T of 0.09 and 0.18 respectively. The simulations were initialized with air at bulk co-flow velocity and at $t = 0$, turbulent inflow were started (Fig. 2). An additional run was perform where the air was initialized with the same turbulent fluctuations as the inflow, the results show little difference. In both cases the fuel was injected at $t = 0$.

Several criterions to detect the ignition process can be found on the literature on this configuration. Experimentally, the auto-ignition length corresponds to the axial location of a 3% rise in the average signal intensity [25] while Galpin et al. [27] use a threshold criterion for OH mass fraction (6.1×10^{-4}). In the present work two approaches have been used to detect the ignition process numerically: OH mass fraction greater than 0.001 and a temperature increase greater than 1% of maximum co-flow temperature. Both methods give the same ignition length (the differences are less than 1%) when the temperature exceeds 2000 K although at lower temperatures, the temperature method predicts earlier ignition. In the random-spots regime, the temperature method is preferred as it detects the kernel formation earlier. In the flash-back regime both methods are nearly undistinguishable Existing chemical mechanisms for complex hydrocarbons involve, typically, more than 1000 elementary reactions and 100 chemical species. The detailed C_1-C_6 sub mechanism for heptane combustion includes 3397 elementary reversible reactions and 781 distinct chemical species [48]. The direct integration of this mechanisms is beyond any present and near future LES computational capabilities. For this reason the reduced mechanism of Liu et al. [49], involving 22 species and 18 reactions, is used. The mechanism originates from a skeletal mechanism of 43 chemical components and 185 reactions, reduced by assuming 21 species to be in steady state. The species for which conservations

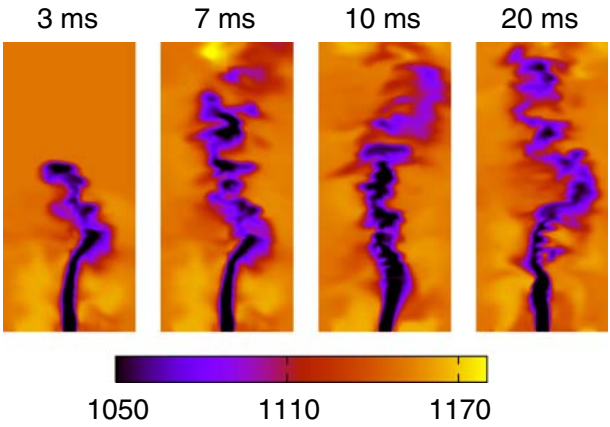

Fig. 2 Snapshots of Temperature distribution at the centre plane for Case 2 (with $T' = 15$ K). The *yellow spot* indicates high temperature auto-ignition spots

equations are explicitly solved are N_2, O_2, H, OH, H_2, H_2O, HO_2, H_2O_2, CO, CO_2, C_2H_2, CH_3, C_2H_4, CH_2O, CH_4, C_3H_4, C_3H_6, C_4H_8, C_6H_{12}, C_7H_{16}, OC_7H_{13} and $C_7H_{15}O_2$.

The simulations were carried out with a constant time step of $\Delta t = 10^{-6}$ s. In a typical run, the maximum velocities are: $\widetilde{\mathbf{u}}_{MAX} \approx 35$ m/s, $\mathbf{u}^g_{max} \approx 30$ m/s and $\mathbf{u}^d_{max} \approx 1$ m/s and the associated Courant number, based on $\left(\widetilde{u}_j + u^g_j + u^d_j\right)_{max}$, is approximately 0.75. The calculations were carried out in a Intel EM64T XEON cluster using 64 nodes and 4 ms of each simulation, takes approximately 3 days (wall time). The maximum mass error, arising from the use of a finite number of stochastic fields, is 0.1%. This error occurs in the vicinity of the inflow boundary, probably due to the discontinuous stochastic velocity. Further downstream, in the region of interest, mass errors are below 0.001%.

4 Results

In the experimental study the term "random spots" was used to describe randomly located ignition kernels that were periodically formed and convected [41, 42, 47]. The same terminology is used in the present study. In the present computational results a different behaviour was observed when the co-flow temperature was varied between 1135 and 1165 K. Both jet and air steams have the same bulk velocities and turbulence effects are expected to be dominated by inflow grid turbulence. At the lowest temperature, $T_{air} = 1135$ K, there was no indication of "auto-ignition". The mean ignition delay time was larger than the flow-through time and no ignition spots were formed. Not enough OH was produced and the maximum heat release is below 50 MW/m^3. At the second temperature investigated, $T_{air} = 1150$ K, the following events can be observed: first, the large carbon chains of n-heptane are broken down in a series of endothermic reactions—see the negative heat release regions in Fig. 3. When the pool of radicals, HO_2, H_2O_2 and heptylperoxil, exceeds a critical value, exothermic reactions dominate and kernels of higher temperature (50–100 K above T_{air}) appear which are convected downstream (see Fig. 2). The influence of the initial conditions disappears after less than about two flow-through

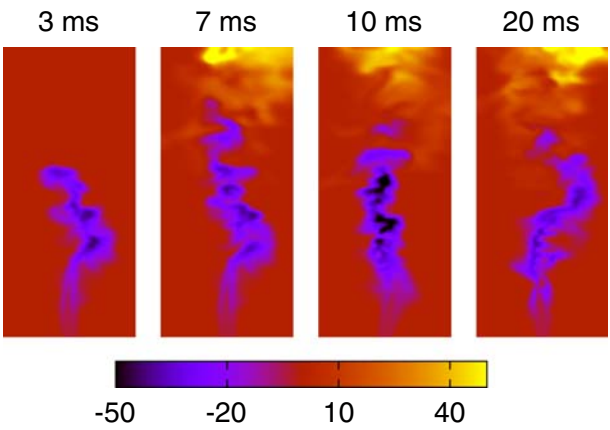

Fig. 3 Snapshots of Heat release MW/m^3 distribution at the centre plane for Case 2 ($T' = 15$ K)

times $\tau_{fl} = L/V_{air} =$ 6.25 ms, with kernels then appearing 'periodically' at roughly the same downstream locations. The time and length scale of these events is clearly dominated by the inflow turbulence, see Fig. 4, a peak in heat release appears periodically every 4.5 ms. Qualitatively, this regime is similar to the "random-spots" observed experimentally.

Increasing the air temperature to 1165 K results in a change in the flame behaviour. The kernels observed at 1150 K (see Fig. 5) merge and flame propagation occurs. This regime was termed "flash-back" in the experiments. The flame exhibit a highly unsteady behaviour and after 10 flow-through times it does not stabilised around a certain lift-off height. The flame propagation speed is not constant, in contrast to that observed in the similar computations using Hydrogen as fuel, and decays from 3 (up to 20 ms) to 1.2 m/s (after 30 ms).

In Fig. 6, the heat release due to combustion, $\dot{q} = -\sum \Delta h_k^0 \dot{\omega}_k$, is shown. The intense heating regions are very thin, approximately 2 or 3 cells and disconnected, in contrast to the peak OH concentration, which suggest a continuous flame front (see Fig. 7). The sub-grid variance of the heat release in the flame front is of the same order

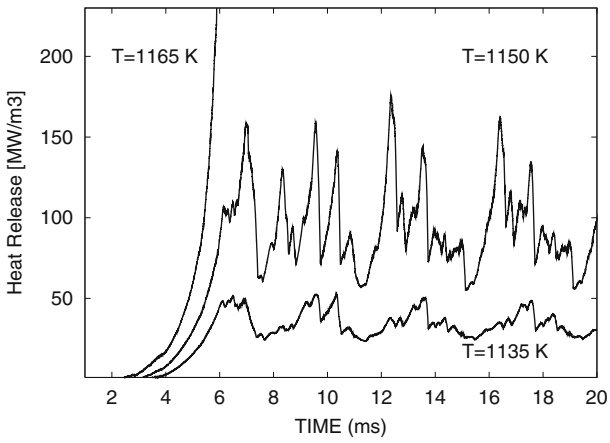

Fig. 4 Maximum heat release, MW/m^3, as a function of time for three temperatures ($T' = 15$ K)

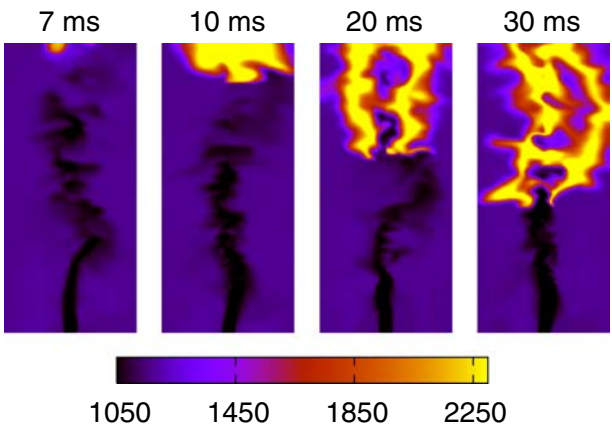

Fig. 5 Snapshots of $\tilde{T}$ distribution at the centre plane for Case 4 ($T' = 15$ K)

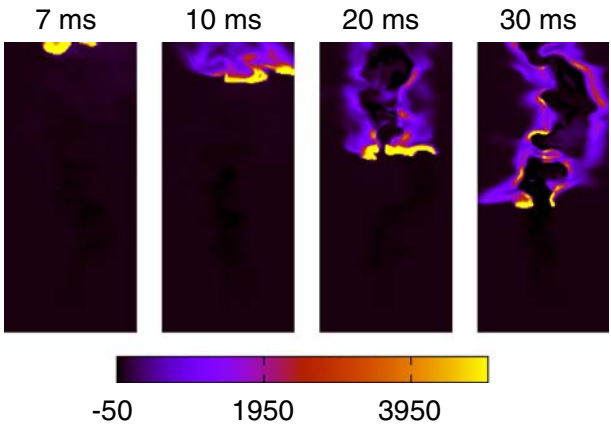

Fig. 6 Snapshots of filtered heat release distribution at the centre plane for Case 4 ($T' = 15$ K)

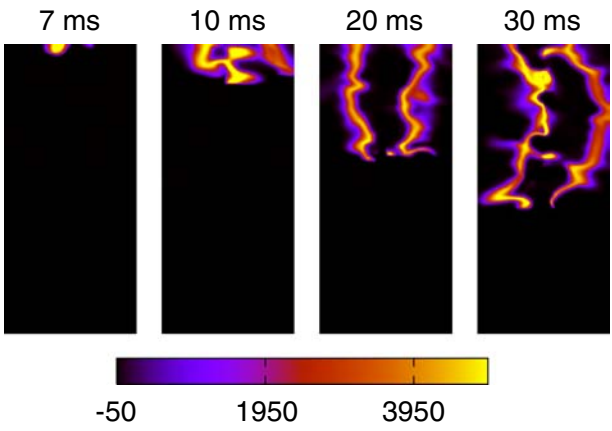

Fig. 7 Snapshots of filtered OH mass fraction distribution at the centre plane for Case 4 ($T' = 15$ K)

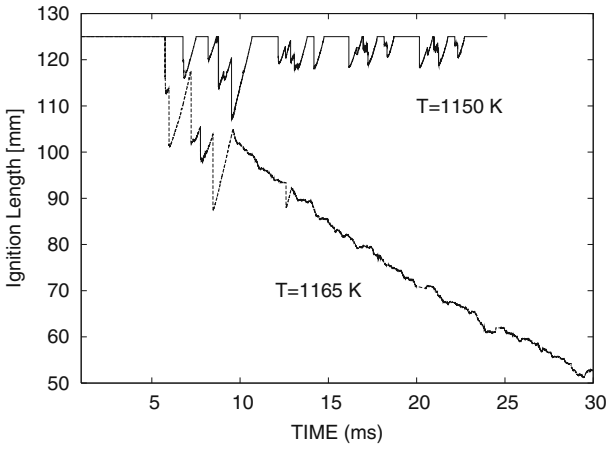

Fig. 8 Ignition length based on $\tilde{T}$ for Cases 2 and 4 (with $T' = 15$ K)

as the filtered value $\dot{q}_{sgs} \approx \widetilde{\dot{q}}$ suggesting a log-normal sub-grid PDF distribution. The complex mixing field pattern allows the existence of pockets of unburnt rich mixture. This is to be contrasted with conventional jet-flames where radial and mixture fraction are highly correlated.

The evolution of ignition length based on temperature is shown in Fig. 8. Case 2 shows a periodicity consistent with the heat release (Fig. 4). The first two kernels appear at 115 and 107 mm, and 'fully developed' state the kernels appear consistently above 117 mm. The flash-back Case 4, has an initial oscillatory period of 4 ms followed by the flash-back regime—unlike the case with $T_{air} = 1165$ K.

The flame behaviour close to the flame base in Case 4 (see Fig. 9) does not lie within the flamelet regime and exhibits large conditional fluctuations respect to mixture fraction, which suggest either extinction due to turbulent stretching or failure to auto-ignite. From a purely premixed point of view, a Karlovitz number of $Ka = \frac{\delta_L u}{\lambda_T u_L}$ can be computed where the laminar burning velocity u_L of n-heptane in air is estimated to be 40 cm/s and the flame thickness in the flame base is

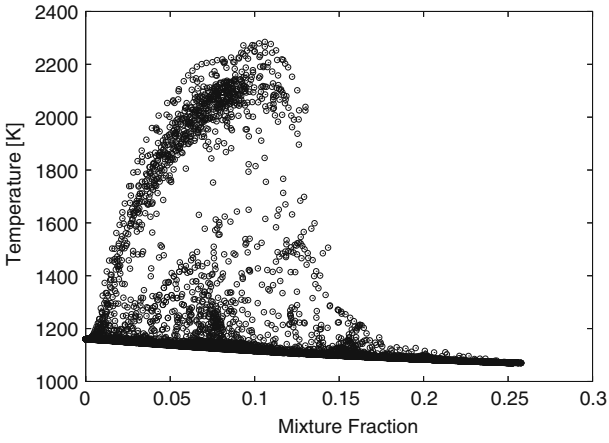

Fig. 9 Scatter plot of temperature as a function of mixture fraction for Case 4 at the flame base ($t = 20$ ms and $x = 87$ mm)

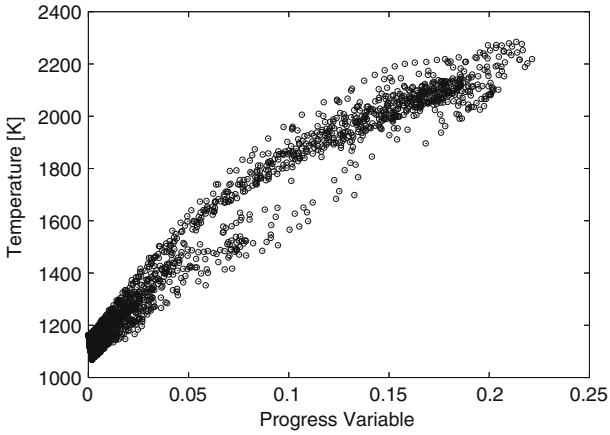

Fig. 10 Scattershot of temperature as a function of progress variable $c = Y_{CO} + Y_{CO2}$ for Case 4 at the flame base

then $\delta_L = 0.2$–0.9 mm using $\delta_L \approx \nu/u_L$, see [50]). The resultant $Ka = 0.2$–$0.6 < 1$ indicates that the premixed flame is in the corrugated flamelets regime in the premixed combustion diagram [51]. However, the existence of large conditional fluctuations in progress variable (see Fig. 10) would infer that the flame behaviour is indeed a combined premixed–diffusion one and specific models for either non-premixed or premixed regimes would not be adequate.

The partially premixed behaviour is also observed at sub-grid level. In Fig. 11, the sub-grid *pdfs* at filter and test filter, $\hat{\Delta} \approx 3\Delta$, are shown. A bi-modal shape can be observed with points at low temperature (not burning) and high temperature (burning) in a region of the size of few Kolmogorov scales, which suggest the presence of a flame front. A wide range of states is present even at the sub-grid level, with temperature fluctuations of nearly 1000 K.

The segregation factor of the mixture fraction, $S_Z = \widetilde{Z''^2}_{sgs}/\tilde{Z}(1-\tilde{Z})$, indicates how well the reactants are mixed at sub-grid level ($S_Z = 0$ for complete mixing and $S_Z = 1$ for totally segregated reactants). Values of $S_Z < 0.01$ were found at the flame base, although values it up to $S_Z \approx 0.2$ were observed in the latter stages of the

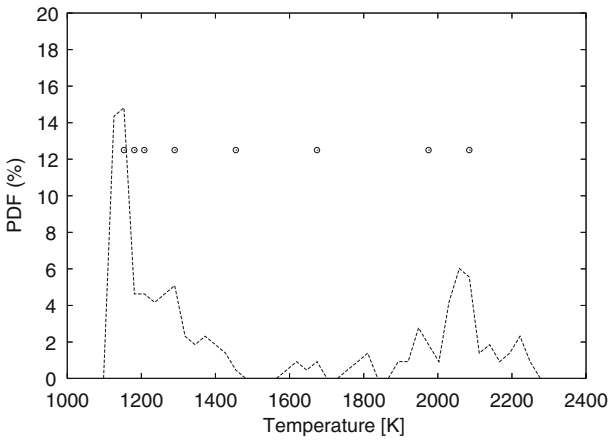

Fig. 11 Sub-grid *pdf* for Case 4 at $t = 20$ ms $x = 87$ mm, $r = 5$ mm and $\theta = 0°$. *Dashed line* is the Sub test-filter *pdf* while the *dots* represents the Sub-filter *pdf*

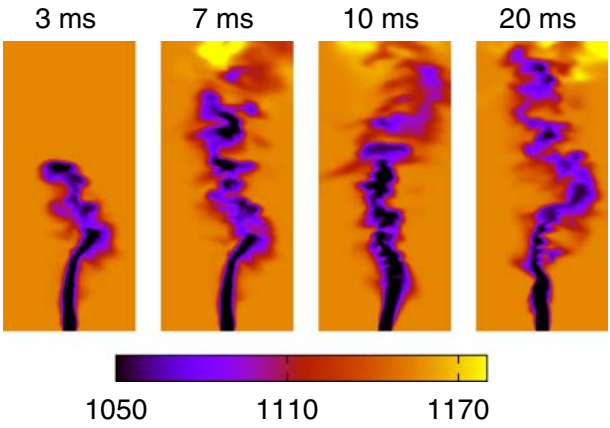

Fig. 12 Snapshots of $\tilde{T}$ distribution at the centre plane for Case 3 with 16 fields

flash-back propagation close to the nozzle. The good degree of mixing at sub-grid level combined with large sub-grid temperature variance at the same location (see Fig. 11), suggests that pre-mixed propagation is the mechanism that controls the flash-back.

Case 3 present characteristics of the "random-spots" regime although the heat release is much larger than Case 2 despite the relatively small 5 K difference in air temperature. A comparison was made for the Case 3 between the results obtained between 8 and 16 fields. Although there is little difference in filtered temperature (Fig. 12, results with 8 fields not shown), discrepancies can be observed (Fig. 13) in the instantaneous sub-grid PDF shapes at the same spatial location. The pdfs are constructed by sampling over the complete cross-section, so that in the case of 16 fields the number of samples is $N_r \times N_\theta \times N = 55296$. When the complete $r - \Theta$ plane is taken into account, the sub-plane *pdfs* are very similar (see Fig. 14), which suggest that the number of fields is sufficient to accurately capture the shape and location of the average *pdfs*.

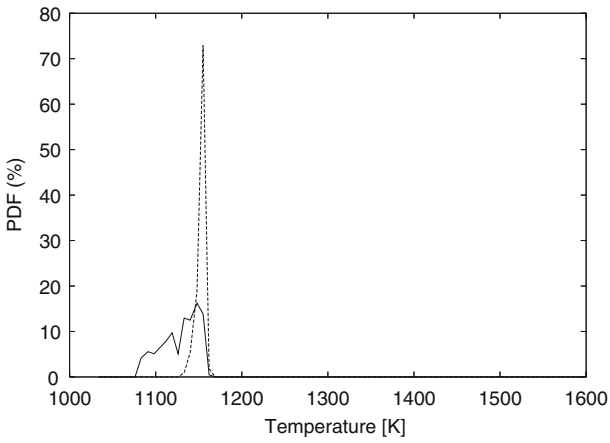

Fig. 13 Sub test-filter PDF for Case 3 with 8 (*solid*) and 16 (*dashed*) fields at $t = 20$ ms, $x = 121$ mm, $r = 3.5$ mm and $\theta = 0°$

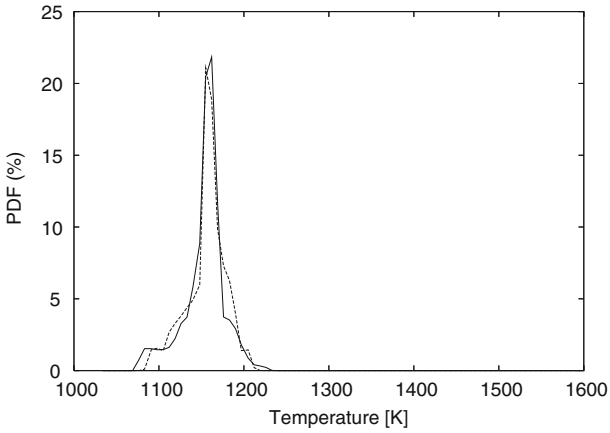

Fig. 14 Sub-Plane PDF for Case 3 with 8 (*solid*) and 16 (*dashed*) fields at $t = 20$ ms and $x = 121$ mm

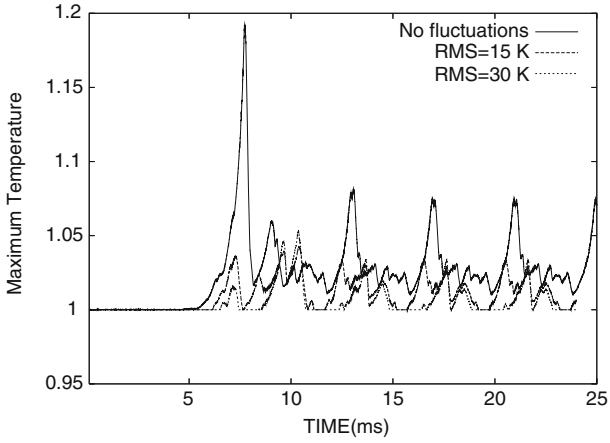

Fig. 15 Maximum relative temperature $\tilde{T}_{max}/\tilde{T}_{max}(t = 0)$) for Case 2 with different temperature fluctuations

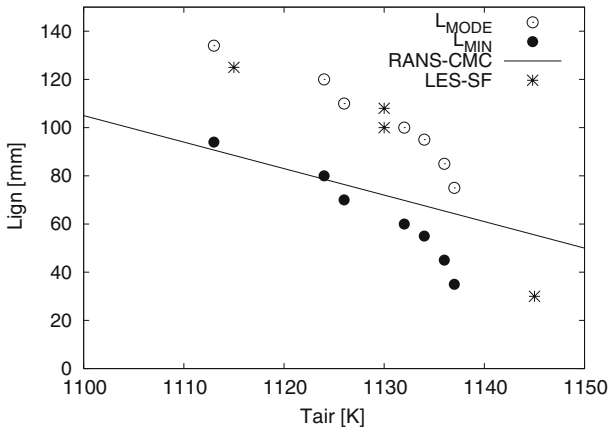

Fig. 16 Comparison of auto-ignition length from experiments (L_{MODE} and L_{MIN}), RANS-CMC predictions [52] and present calculations (shifted 20 K)

The effect of temperature fluctuations was surprisingly large, even with a relatively small fluctuation of 15 K (less than 2%). The maximum temperature obtained with the same mean co-flow temperature and three different RMS values is shown in Fig. 15. With no temperature fluctuations a maximum temperature of 1370 K is obtained and $\dot{q}_{max} = 900\,\mathrm{MW/m^3}$. The introduction of fluctuations reduces the strength of the ignition kernels and maximum temperatures of 1215 and 1240 K are obtained with $\dot{q}_{max} \approx 200\,\mathrm{MW/m^3}$. The minimum ignition length is roughly 10 mm shorter.

In Fig. 16 the ignition length observed in the experiments (minimum and mode) are shown compared with previous RANS-CMC results [52] and present simulations. As observed there is large difference between the most probable occurrence of ignition kernels, L_{MODE}, and the minimum ignition length L_{MIN}. If present simulations are shifted 20 K the results fitted well with the mode ignition length. The exception is Case 4, which is not in the "random-spots" regime and therefore cannot be directly compared.

5 Conclusions

This paper represents one of the first attempts to resolve auto-ignition phenomena in realistic fuels using LES. All regimes captured in the experiments were observed in our simulations without any adjustment or calibration of the model constants. The results are consistent with experimental data and previous RANS calculations. Discrepancies can be attributed to uncertainties in temperature fluctuations in the inflow stream and the chemical mechanism. The method is able to capture the partially premixed behavior even at sub-grid level, which makes it very attractive for complex combustion problems. The inclusion of temperature fluctuations in the system reduced the progress rate of combustion and delays the formation of auto-ignition kernels. Relatively moderate temperature fluctuations of 2% in the co-flow decrease the maximum temperatures in more than 10%. The sensitivity of the system to temperature fluctuations is probably due to the slow rate of formation of R-HO_2 and R-H_2O_2 at low temperature. The formation of these intermediate species can be easily disrupted as the chemical time scales are comparable to the flow time scales and noise in the temperature field affect directly the rate of production.

Acknowledgement The authors would like to acknowledge the financial support provided by EPSRC under Platform Grant EP/C518101/1.

References

1. Blouch, J.D., Law, C.K.: Effects of turbulence of non-premixed ignition of hydrogen in heated counterflow. Combust. Flame **132**, 512–522 (2003)
2. Mastorakos, E., Baritaud, T.A., Poinsot, T.J.: Numerical simulations of autoignition in turbulent mixing flows. Combust. Flame **109**, 198–223 (1997)
3. Cao, S., Echekki, T.: Auto-ignition in nonhomogeneous mixtures: conditional statistics and implications for modeling. Combust. Flame **151**, 120–141 (2007)
4. Lawn, C.J.: Lifted flames on fuel jets in co-flowing air. Prog. Energy Combust. Sci. **35**, 1–30 (2009)
5. Pierce, C.D., Moin, P.: A dynamic model for subgrid variance and dissipation rate of a conserved scalar. Phys. Fluids **10**(12), 3041–3044 (1998)

6. Branley, N., Jones, W.P.: Large eddy simulation of a turbulent non-premixed flame. Combust. Flame **127**, 1914–1934 (2001)
7. Pitsch, H., Steiner, H.: Large-eddy simulation of a turbulent piloted methane/air diffusion flame (Sandia flame D). Phys. Fluids **12**, **10**, 2541–2554 (2000)
8. Navarro-Martinez, S., Kronenburg, A., di Mare, F.: Conditional moment closure for large eddy simulations. Flow Turbul. Combust. **75**, 245–274 (2005)
9. Hawkes, E.R., Cant, R.S.: A flame surface density approach to large-eddy-simulation of premixed turbulent combustion. Proc. Combust. Inst. **28**, 51–58 (2000)
10. Huang, Y., Sung, H., Hsieh, S., Yang, V.: Large-eddy simulation of combustion dynamics of lean-premixed swirl-stabilized combustor. J. Propuls. Power **19**(5), 782–794 (2003)
11. Pitsch, H.: A consistent level set formulation for large-eddy simulation of premixed turbulent combustion. Combust. Flame **143**, 587–598 (2005)
12. Pitsch, H.: Large eddy simulations of turbulent combustion. Annu. Rev. Fluid Mech. **38**, 453–482 (2006)
13. Gao, F., O'Brien, E.: A large eddy simulation scheme for turbulent reacting flows. Phys. Fluids, A **5**, 1282–1284 (1993)
14. Raman, V., Pitsch, H., Fox, R.O.: Hybrid large-eddy simulation/lagrangian filtered density function approach for simulating turbulent combustion. Combust. Flame **143**, 56–78 (2005)
15. Raman, V., Pitsch, H.: A consistent les/filtered-density function formulation for the simulation of turbulent flames with detailed chemistry. Proc. Combust. Inst. **31**, 1711–1719 (2007)
16. Valiño, L.: A field Monte carlo formulation for calculating the probability density function of a single scalar in a turbulent flow. Flow Turbul. Combust. **60**, 157–172 (1998)
17. Sabel'nikov, V., Soulard, O.: Rapidly decorrelating velocity-field model as a tool for solving one-point fokker-planck equations for probability density functions of turbulent reactive scalars. Phys. Rev., E **72**, 016301–016322 (2005)
18. Mustata, R., Valiño, L., Jimenez, C., Jones, W.P., Bondi, S.: A probability density function eulerian monte carlo field method for large eddy simulations. Application to a turbulent piloted methane/air diffusion flame. Combust. Flame **145**, 88–104 (2006)
19. Jones, W.P., Navarro-Martinez, S.: Large eddy simulation of auto-ignition with a subgrid probability density function. Combust. Flame **150**, 170–187 (2007)
20. Gkagkas, K., Lindstedt, R.P.: Transported PDF modelling with detailed chemistry of pre and auto-ignition in Ch4/air mixtures. Proc. Combust. Inst. **31**, 1559–1586 (2007)
21. Cabra, R., Chen, J.Y., Dibble, R.W., Karpetis, A.N., Barlow, R.S.: Lifted methane-air jet flames in vitiated coflow. Combust. Flame **143**, 491–506 (2005)
22. Masri, A.R., Cao, R., Pope, S.B., Goldin, G.M.: Pdf calculations of turbulent lifted flames of h2/n2 fuel issuing into a vitiated co-flow. Combust. Theory Model. **8**, 1–2 (2004)
23. Domingo, P., Vervisch, L., Veynante, D.: Large-eddy simulation of a lifted methane flame in a vitiated coflow. Combust. Flame **152**, 415–432 (2008)
24. Navarro-Martinez, S., Kronenburg, A.: Les-cmc simulations of a methane lifted flame. Proc. Comb. Inst. **32**, 1509–1516 (2009)
25. Paola, G.D., Kim, I.S., Mastorakos, E.: Second-order conditional moment closure simulations of autoignition of an n-heptane plume in a turbulent coflow of heated air. Flow Turbul. Combust. doi:10.1007/s10494-008-9183-x (2008)
26. Lee, C.W., Mastorakos, E.: Transported scalar pdf calculations of autoignition of a hydrogen jet in a heated turbulent co-flow. Combust. Theory Model. **12**, 1153–1178 (2008)
27. Galpin, J., Angelberger, C., Naudin, A., Vervisch, L.: Large-eddy simulation of h2-air auto-ignition using tabulated detailed chemistry. J. Turbul. **9**(13), 1–21 (2008)
28. Jones, W.P., Navarro-Martinez, S.: Study of hydrogen auto-ignition in a turbulent air co-flow using a large eddy simulation approach. Comput. Fluids **37**, 802–808 (2008)
29. Smagorinsky, J.: General circulation experiments with the primitive equations. Mon. Weather Rev. **91**, 99–164 (1963)
30. Piomelli, U., Liu, J.: Large eddy simulation of rotating channel flows using a localized dynamic model. Phys. Fluids **7**(4), 893–848 (1995)
31. Colucci, P.J., Jaberi, F.A., Givi, P., Pope, S.B.: Filtered density function for large eddy simulation of turbulent reacting flows. Phys. Fluids **10**, 499–515 (1998)
32. Jaberi, F.A., Colucci, P.J., James, S., Givi, P., Pope, S.B.: Filtered mass density function for large-eddy simulation of turbulent reacting flows. J. Fluid Mech. **401**, 85–121 (1999)
33. Schmidt, H., Schumann, U.: Coherent structure of the convective boundary layer derived from large eddy simulation. J. Fluid Mech. **200**, 511–562 (1989)

34. Fox, R.O.: Computational Models for Turbulent Reacting Flows. Cambridge University Press, Cambridge (2003)
35. Villermaux, J., Devillon, J.C.: Représentation de la redistribution des domaines de ségrégation dans un fluide par un modéle dinteraction phénoménologique. In: Proceedings of the Second International Symposium on Chemical Reaction Engineering. Elsevier, Amsterdam (1972)
36. Dopazo, C., O'Brien, E.: Functional formulation of nonisothermal turbulent reactive flows. Phys. Fluids **17**(11), 1968–1975 (1974)
37. Dopazo, C.: Probability density function approach for an axisymmetric heated jet: centerline evolution. Phys. Fluids **18**, 397–404 (1975)
38. Jones, W.P., Navarro-Martinez, S., Rohl, O.: Large eddy simulation of hydrogen auto-ignition with a probability density function method. Proc. Comb. Inst. **31**, 1765–1771 (2007)
39. Kloeden, P.E., Platen, E.: Numerical Solution of Stochastic Differential Equations, English edn. Springer, New York (1992). ISBN 3-540-54062-8
40. Gardiner, C.: Handbook of Stochastic Methods, English edn. Springer-Verlag, New York (1985)
41. Markides, C.N., Mastorakos, E.: An experimental study of hydrogen auto-ignition in a turbulent co-flow of heated air. Proc. Combust. Inst. **30**, 883–891 (2005)
42. Markides, C.N., Paola, G.D., Mastorakos, E.: Measurements and simulations of mixing and auto-ignition of an n-heptane plume in a turbulent flow of heated air. Exp. Therm. Fluid Sci. **31**, 393–401 (2007)
43. Jones, W.P., di Mare, F., Marquis, A.J.: LES-BOFFIN: Users Guide. Technical Memorandum, Imperial College, London (2002)
44. Branley, N., Jones, W.P.: Large eddy simulation of turbulent flames. In: CD-Rom Proceedings. ECCOMAS, Barcelona (2000)
45. Van Leer, B.: Towards the ultimate conservative difference scheme. II. Monotonicity and conservation combined in a second order scheme. J. Comput. Physics **14**, 361–370 (1974)
46. di Mare, L., Klein, M., Jones, W.P., Janicka, J.: Synthetic turbulence inflow conditions for large eddy simulation. Phys. Fluids **18**, 025107–025118 (2006)
47. Markides, C.N., Mastorakos, E.: Flame propagation following the autoignition of axisymmetric hydrogen, acetylene, and normal-heptane plumes in turbulent coflows of hot air. J. Eng. Gas Turbines Power-Trans ASME **130**(1). doi:10.1115/1.2771245 (2008) (51st ASME Turbo Expo, Barcelona, SPAIN, 6–11 May 2006)
48. Westbrook, C.K., Pitz, W.J., Boercker, J.E., Curran, H.J., Griffiths, F., Mohamed, C., Ribaucour, M.: Detailed chemical kinetic reaction mechanisms for autoignition of isomers of heptane under rapid compression. Proc. Combust. Inst. **29**, 1311–1318 (2002)
49. Liu, S., Hewson, J.C., Chen, J.H., Pitsch, H.: Effects of strain rate on high-pressure non-premixed n-heptane auto-ignition in counterflow. Combust. Flame **137**, 320–339 (2004)
50. Cant, R.S., Mastorakos, E.: An Introduction to Turbulent Reacting Flows. Imperial College Press, London (2008)
51. Peters, N.: Turbulent Combustion. Cambridge University Press, Cambridge (2000)
52. Paola, G.D., Kim, I.S., Mastorakos, E.: Second order conditional moment closure simulations of auto-ignition of an n-heptane plume in a turbulent coflow of heated air. In: ECCOMAS, Computational Combustion Symposium (2007)